Int. J. Heat Mass Transfer. Vol. 31, No. 11, pp. 2215–2225, 1988
Printed in Great Britain

0017–9310/88 $3.00+0.00

Fundamental study of heat transfer and flow situation around a spacer (in the case of a cylindrical rod as a spacer)

KOICHI ICHIMIYA
Department of Mechanical Engineering, Yamanashi University, Takeda-4, Kofu, Yamanashi 400, Japan

NORIO AKINO and TOMOAKI KUNUGI
Japan Atomic Energy Research Institute, Tokai-mura, Nakagun, Ibaragi 319-11, Japan

and

KOJI MITSUSHIRO
Matsushita Electric Industry Co., Ltd., Kadoma, Ohsaka 571, Japan

(*Received* 9 *October* 1987 *and in final form* 17 *November* 1987)

Abstract—This paper describes the heat transfer augmentation and the flow situation around a single spacer (a cylindrical rod) on the heated surface of a parallel plate duct in order to examine basically the effects of the spacer in the fuel elements of a high temperature gas-cooled reactor. The ends of the cylindrical rod contact the upper and lower planes. A thermosensitive liquid crystal film is used to indicate the effective area for the heat transfer. The mean Nusselt number, which is estimated within the optional distance from the spacer to the downstream direction, peaks at a dimensionless distance of $X/D = 1$–3, and after that decreases gradually with the flow direction. The manner in which heat transfer corresponds to the flow situation is also examined. The horseshoe vortex, produced around the spacer, affects the wake and contributes to the increase of the local heat transfer.

INTRODUCTION

IN THE fuel elements of a high temperature gas-cooled reactor, helium gas flows as a coolant through a narrow space between fuel rods and between a fuel rod and a moderator. In order to support these narrow spaces, several ribs are placed on the circumferential or longitudinal surface of fuel rods. However, the manner in which the spacer affects the flow and the local heat transfer has not been examined. Therefore, the effects of spacers on the local heat transfer and the flow situation should be examined in detail.

Some experimental studies have been performed on three-dimensional flow and local heat transfer on the surface of a rib [1] or on augmentation heat transfer by separation and reattachment of flow [2]. In addition, the effects of circular cylinders set in the perpendicular direction to the flow on the center of a parallel plate duct have been examined experimentally with the local heat transfer and flow situation by changing the blockage ratio (the ratio of the outer diameter of a circular cylinder and the width of the flow passage) [3–5]. However, effects of the ribs have not been studied in the system where a rib is placed through the whole height of the flow passage like a spacer.

In the present study, a cylindrical rod was set vertically to the flow direction from the upper plate to the lower one of a parallel plate duct, and the effects of the rod as a spacer were examined experimentally. A liquid crystal sheet was placed on a heater in order to examine the effective local heat transfer and to visualize the temperature distribution. The flow situation around the spacer was also observed using a water circulation system. In addition, correspondence between the flow and the heat transfer was examined.

EXPERIMENTAL FACILITY AND PROCEDURE

Experimental facility

A schematic diagram of the experimental facility is shown in Fig. 1. The test section was set on the suction

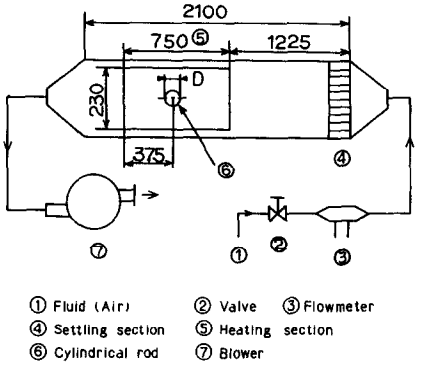

FIG. 1. Schematic diagram of the experimental facility for heat transfer.

NOMENCLATURE

D	outer diameter of a cylindrical rod	Re	Reynolds number, UD_H/ν
D_H	hydraulic diameter, $2H$	T	temperature
H	distance between the upper and lower planes	X	longitudinal distance from the end of a cylindrical rod
Nu	Nusselt number, $\alpha D_H/\lambda$	Y	lateral distance from the center of a cylindrical rod.
Nu_m	average Nusselt number		
Nu_{max}	maximum Nusselt number		
Nu_∞	thermally fully developed Nusselt number for a parallel plate duct with one side heated	Greek symbols	
		α	local heat transfer coefficient
q	heat flux	λ	thermal conductivity
		ν	kinematic viscosity.

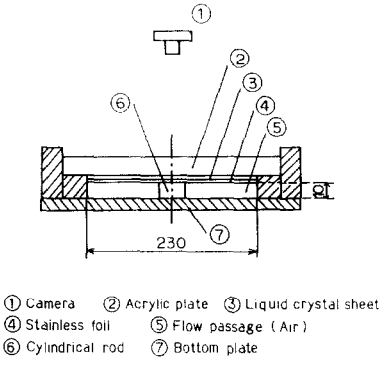

FIG. 2. Cross-sectional view of the test section.

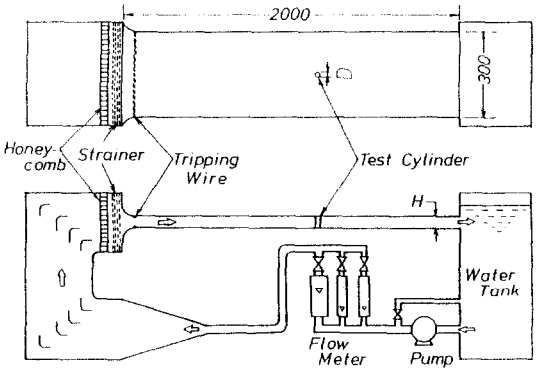

FIG. 3. Recirculating water bath for flow visualization.

side of a blower and was composed of a parallel plate duct of which the width, length and height were 230, 2100 and 10 mm, respectively. After the air flowed through the control valve ②, the flow meter ③ and the settling section ④, it was heated uniformly in the heating section ⑤ and returned to the atmosphere via the blower. A cylindrical rod ⑥ was set at a point 375 mm from the end of the heating section (1600 mm from the entrance of the settling section). The cylindrical rod was placed between the upper and lower plates of the parallel plate duct and was attached using silicon grease of thickness 0.01 mm. The liquid crystal layer and stainless steel foil were adhered to the upper plate of the duct which was made of transparent acrylic resin (Fig. 2).

Table 1. Relation between color and temperature

Color boundary	Temperature (°C)
Black–dark brown	26.0±0.2
Dark brown–light brown	27.1±0.2
Light brown–orange	28.3±0.2
Orange–yellow	29.8±0.5
Yellow–yellow green	30.7±0.6
Yellow green–green	31.3±0.4
Green–light blue	32.3±0.5
Light blue–dark blue	35.6±0.4

Stainless steel foil, the thickness and length of which were 0.05 and 750 mm, respectively, composed the heating section and was heated uniformly by controlling the alternating current of 100 V.

The thermosensitive liquid crystal layer was used to measure the temperature distribution in the effective area of the cylindrical rod. The cholesteryl-type capsuled liquid crystal layer [6] was used because it has a long life span. It changes to eight different colors which depends on the temperature. A liquid crystal sheet the width and length of which were 230 and 750 mm, respectively, was composed of a thermosensitive liquid crystal layer and a black adhesive layer. The relationship between its color and temperature was determined by a calibration test and is shown in Table

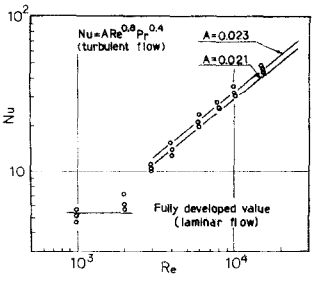

FIG. 4. Nusselt number in a smooth parallel plate duct (one side heated and the other side insulated).

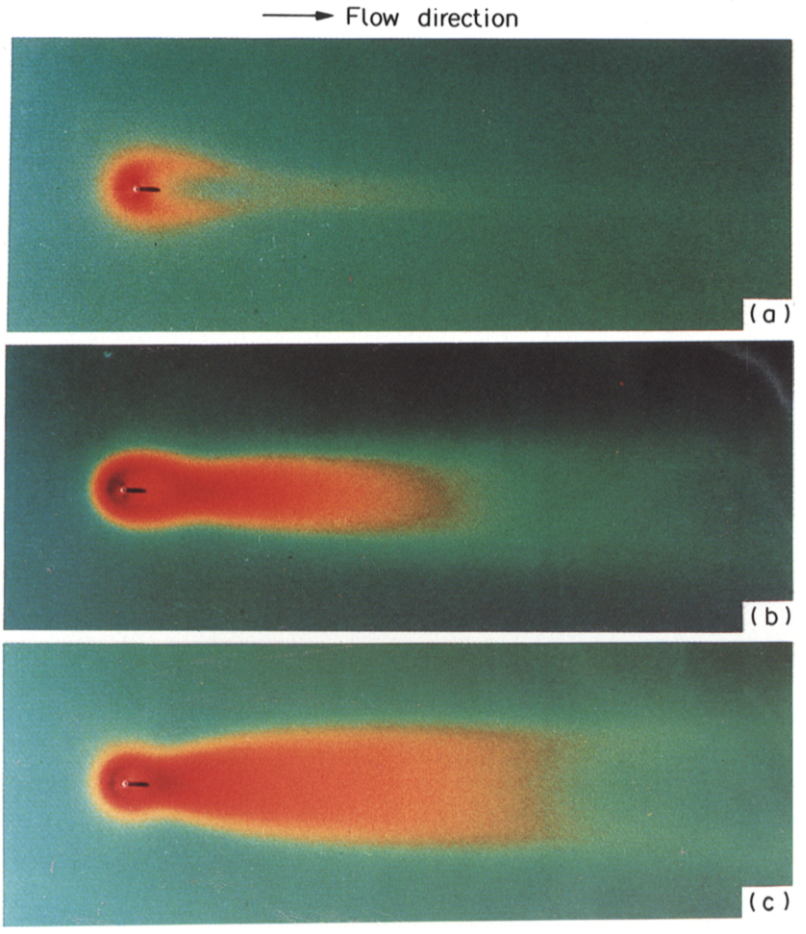

FIG. 5. Isothermal distribution around a cylindrical rod (liquid crystal sheet) (an acrylic resin cylindrical rod with $D = 10$ mm): (a) $Re = 1000$; (b) $Re = 4000$; (c) $Re = 10000$.

1. The relation was obtained by setting a given linear temperature gradient on a heated plate for calibration [7]. The colors of this liquid crystal were black, dark brown, light brown, orange, yellow, yellow–green, green, light blue and dark blue in a temperature range from 26 to 36°C.

A water-recirculating bath was used to visualize the flow pattern around a cylindrical rod (Fig. 3). A cylindrical rod, the outer diameter of which was 20 mm, was set in the center of the flow passage of width 300 mm and height 20 mm. Small pearlized particles (diameter, 30 μm; specific weight, 3) made of mica and covered with titanium oxide [8], were traced in the water flow. These particles reflect light well. Through this inspection, the shearing direction of the flow made it possible for the flow to be visualized by illuminating the slit (width, 1 mm) of a light source.

Experimental procedure

In the first stage, the heat transfer experiment was performed on a smooth parallel plate duct (one side heated and the other side insulated) without a cylindrical rod.

In the second stage, a cylindrical rod had been set, and the alternating current was charged to the stainless steel foil. The surface temperature was maintained within the thermosensitive region of the liquid crystal controlling the electric current and voltage. Entrance and exit temperatures of air were measured directly by thermocouples. The mixed mean temperature, T_b, of the air at an arbitrary point was estimated by assuming a linear longitudinal distribution of the air temperature. The maximum difference between the net heat flow and the electric input was 7%. The surface temperature, T_w, was measured by converting the color of the liquid crystal sheet into the temperature. The local heat transfer coefficient was obtained by the following equation:

$$\alpha = q/(T_w - T_b) \tag{1}$$

where q is the local heat flux. The scattering of the local heat transfer coefficient was about $\pm 10\%$ including the errors in the surface and fluid temperature measurements.

The present experiments were carried out using 10 mm high cylindrical rods for three different outer diameters of $D = 10$, 15 and 20 mm with two materials, acrylic resin and brass. The Reynolds number with a characteristic length of $2H$ changed from 1000 to 10000.

RESULTS AND DISCUSSIONS

Heat transfer for a smooth parallel plate duct

Figure 4 represents the experimental results of a smooth parallel plate duct. The ordinate shows the most developed Nusselt number, Nu, and the abscissa denotes the Reynolds number, Re. These values were obtained at the position corresponding to the cylindrical rod and in the most developed hydraulic and thermal conditions. They agree well with the fully developed value [9], and their scattering is within $\pm 10\%$ in the turbulent region. On the other hand, in the laminar region, the experimental values are equal to the analytical value $Nu = 5.4$ [10] at $Re = 1000$. However, at $Re = 2000$, these are larger than the analytical values because they are in the transition region.

Heat transfer around a single cylindrical rod

Figure 5 shows the temperature distribution around a cylindrical rod (outer diameter $D = 10$ mm) made of acrylic resin on a liquid crystal sheet for $Re = 1000$, 4000 and 10000. A uniform color of the liquid crystal indicates an isothermal situation. A stagnation region exists behind the cylindrical rod at $Re = 1000$. Therefore, the temperature increases in this region. As Re increases, the local heat transfer is improved in the downstream region since two separated flows are joined after the cylindrical rod. Additionally, the position of the depression of the isothermal domain downstream of the cylindrical rod tends to approach the rod (move toward the upstream region).

Figure 6 shows the iso-Nusselt number lines obtained by local temperature distribution and equation (1) with dimensionless distance (X/D is the distance from the cylindrical rod edge and Y/D the lateral distance from the center line of a cylindrical rod) for three Reynolds numbers. For a cylindrical rod made of acrylic resin, the maximum Nusselt number exists before stagnation occurs behind the cylindrical rod at $Re = 1000$. On the other hand its position is on the symmetric line of the center axis of the cylindrical rod at high Reynolds numbers (turbulent region). The region where local heat transfer is clearly improved is less than $X/D = 5$ for $Re = 1000$ and is more than double, $X/D = 11$, for $Re = 10000$. However, slight differences in the colors of the liquid crystal sheet exist symmetrically in the downstream region, $X/D \geqslant 20$.

While a cylindrical rod made of acrylic resin is in contact with the heat transfer surface at the insulated condition due to low thermal conductivity (0.194 W m^{-1} K^{-1}), a cylindrical rod made of brass produces the fin effect (extended surface) because of high thermal conductivity (98.9 W m^{-1} K^{-1}). As a result, a maximum Nusselt number exists on the periphery of the rod as shown in Fig. 6(d). This local maximum value is larger than that of the acrylic resin. The effective area of heat transfer, however, does not depend on the material of the cylindrical rod.

Effects of the dimension of the outer diameter on heat transfer do not appear clearly at constant Reynolds numbers. The absolute value of the effective area increases with the diameter of the cylindrical rod. Iso-Nusselt number lines are expressed similarly by using dimensionless distances X/D and Y/D.

Figure 7 shows a comparison with the results of other research. The comparison is based on the Nusselt number ratio, Nu/Nu_∞, normalized by the fully developed value. The upper half contours of the figure show the present results and the lower half Goldstein

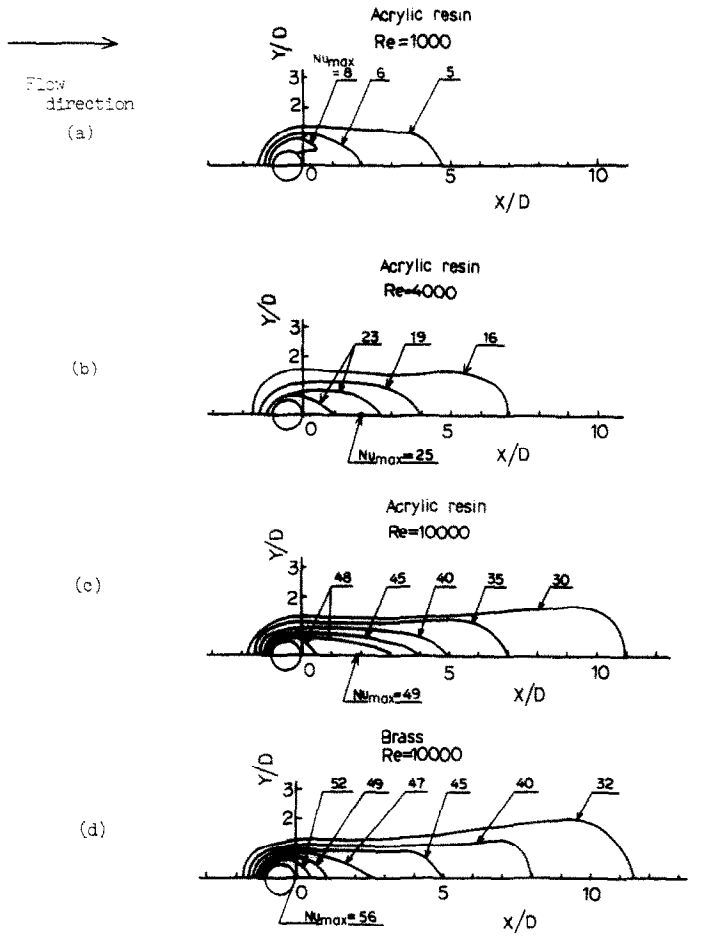

FIG. 6. Local Nusselt number (D = 10 mm).

et al.'s results [11] which were obtained for a three-dimensional circular rod. The local heat transfer of ref. [11] reaches a peak at the reattached region since fluid flows over the head of the rod and reattaches to the heat transfer surface. However, the effective area for heat transfer is similar to the present result.

Improvement of heat transfer is generally evaluated by (i) the maximum Nusselt number ratio, Nu_{max}/Nu_{∞} or (ii) the average Nusselt number ratio, Nu_m/Nu_{∞}, where Nu_{∞} is a fully developed value for a smooth parallel plate duct. Ratio (i) shows a maximum evaluation. While the average value of the whole effective area of a cylindrical rod has been used up to this time, in the evaluation of ratio (ii), the most effective area was determined by obtaining Nu_m/Nu_{∞} for an arbitrary distance from the edge of a cylindrical rod. Figure 8 shows a model to estimate Nu_m/Nu_{∞} from Fig. 6. The average value Nu_m/Nu_{∞} was obtained by multiplying Nu_k and A_k and averaging the entire area

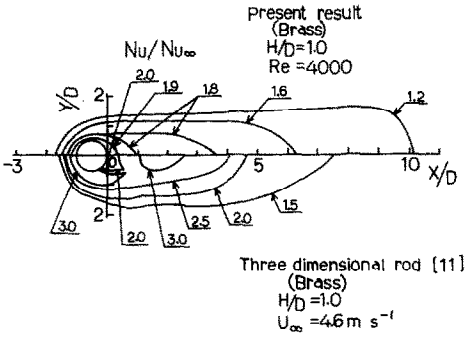

FIG. 7. Local Nusselt number ratio.

$$Nu_m/Nu_{\infty} = \left(\sum_{k=1}^{N-1}(Nu_{k+1}-Nu_k)A_{k+1}+Nu_1A_1\right)\Big/ Nu_0A_1 \quad (2)$$

where Nu_k is the iso-Nusselt number value for the arbitrary distance from a cylindrical rod and A_k the area of Nu_k. These results are shown in Figs. 9 and 10.

In Fig. 9, the relationship between Nu_{max}/Nu_{∞} and Re is shown for acrylic resin and brass. After Nu_{max}/Nu_{∞} increases with Re in the laminar region

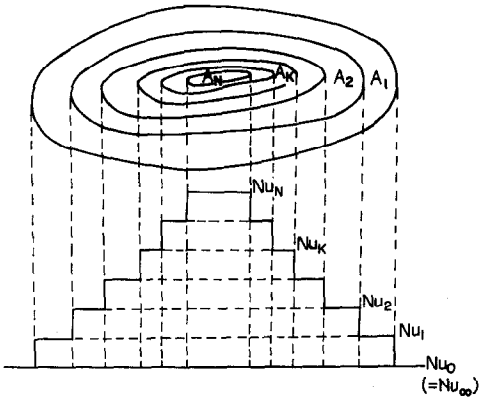

FIG. 8. A model of the local Nusselt number distribution.

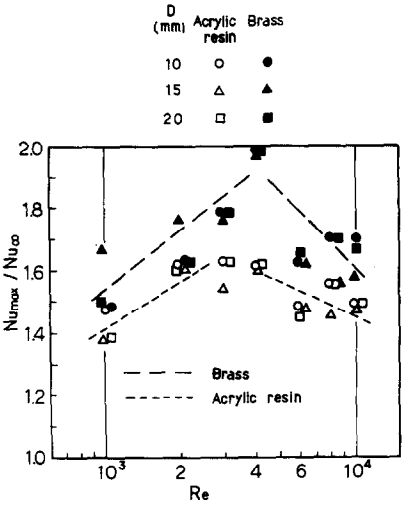

FIG. 9. Maximum Nusselt number.

and reaches a peak at $Re = 3000$–4000, it then tends to decrease in the turbulent region. In the case of acrylic resin, the maximum Nusselt number is expressed by Re^n the index of which is $n = 0.66$. Zemanick and Dougall [12] obtained the index $n = 2/3$ and Filleti and Kays [13] $n = 0.593$–0.689 for the Reynolds number index for the maximum Nusselt number on the reattached region of an abruptly extended flow. For heat transfer of the side surface of a finite circular cylinder on a smooth plate [1], the index $n = 0.657$, in which the ratio of the outer diameter and height is 1. It is interesting that these values are similar to our results ($n = 0.66$). The maximum Nusselt number of the brass cylinder is about 25% higher than that of the acrylic resin cylinder at $Re = 4000$, because of the high thermal conductivity, namely the fin effect.

Figures 10(a) and (b) represent the relationship between the average Nusselt number Nu_m/Nu_∞ and the dimensionless distance X/D as a parameter of Re. In Fig. 10(a), the effects of the acrylic cylinder appear before the stagnation region around the cylinder for low Reynolds numbers. While Nu_m/Nu_∞ reaches a peak at $X/D = 1$–2 for $Re = 1000$ and 2000, the peak moves to $X/D = 3$ for $Re = 10\,000$. The value approaches 1 at the downstream region. In the figure, the representative tendency is shown with a dashed line. Effects of the outer diameter do not appear clearly in the behavior. In Fig. 10(b), Nu_m/Nu_∞ reaches a peak at $X/D = 1$ for all Reynolds numbers in the experiment and also approaches 1 along the downstream region.

These facts will be useful as fundamental data to determine a longitudinal pitch when several spacers are to be set in a flow passage.

Flow situation

The flow situation around a cylindrical rod was visualized corresponding to the local heat transfer by using a water recirculating bath. The results represent that the flow is mainly characterized by a wake flow behind a cylindrical rod and horseshoe vortices around a rod.

Figures 11(a)–(c) are photographs taken by illuminating horizontally the slit of a light source. These Reynolds numbers are $Re = 1000$, 4000 and 10 000. The stagnation flow is in the upstream region. Separation flow on the side surface and wake flow are

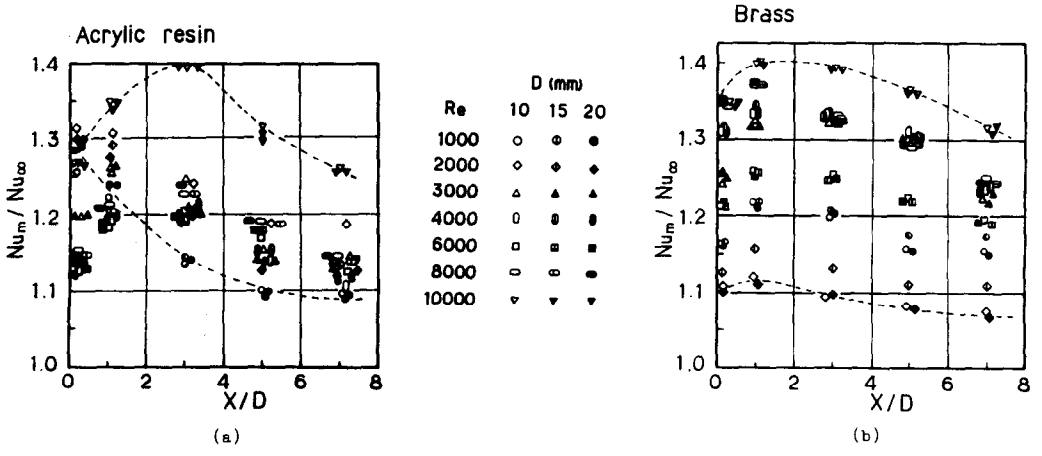

FIG. 10. Average Nusselt number.

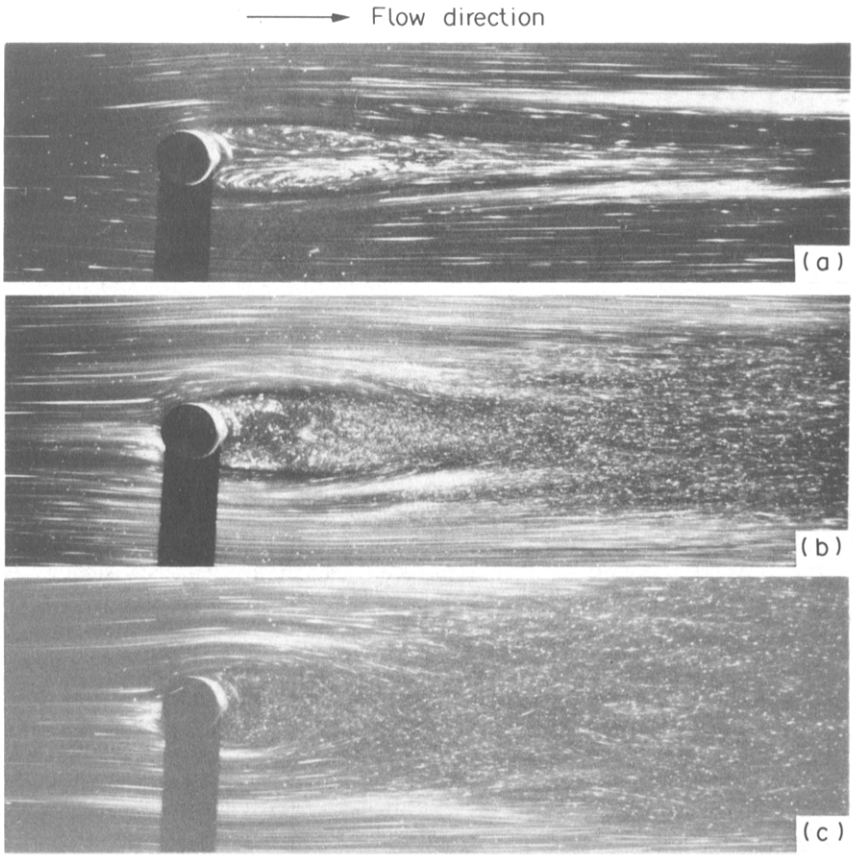

FIG. 11. Main stream line at half height from the bottom plate (exposure, f1.4; time, 0.5 s): (a) $Re = 1000$; (b) $Re = 4000$; (c) $Re = 10000$.

observed in all the photographs and are similar to the flow around a long cylindrical rod. The wake flow depends on Re and is classified into a stagnation flow following the cylindrical rod and a wake region. Stable twin vortices are constructed in the stagnation region for a Reynolds number less than $Re = 1500$ and their tails extend longitudinally. The flow is stable and is considered to be laminar. The blue color of the liquid crystal sheet corresponds to the stagnation region and the temperature is comparatively high (Fig. 5(a)).

For Reynolds numbers higher than $Re = 1500$, the tail of twin vortices is irregular and the area of the stagnation region is reduced. A disturbed wake region appears downstream of the stagnation region, and the width extends along the downstream region for Reynolds numbers higher than $Re = 2000$. Alternate vortices (similar to Karman vortices) are generated for Reynolds numbers higher than $Re = 4000$, but these disappear in a disturbed wake region under $Re = 6000$. The maximum Nusselt number Nu_{max}/Nu_{∞} reaches a peak in the range of the above-mentioned Reynolds number (refer to Fig. 9). Alternate vortices did not appear owing to the slow shutter speed of the camera; the flow was normalized during exposure. Alternate vortices were clearly observed by adding a solution of pearlized particles. These vortices were generated for Reynolds numbers higher than those in which normal Karman vortices were produced. Three-dimensional constructions of these flows were not clear in the present study.

Flow around a cylindrical rod was also observed from the side surface of the flow passage by illuminating vertically the slit of a light source from an upper direction and using an amplifier. Fluid collided with the rod and caused several horseshoe vortices [14] which surrounded the base of a cylindrical rod and washed out to the downstream region. The behavior of horseshoe vortices is shown schematically in Figs. 12(a)–(c). Two stable horseshoe vortices were observed for Reynolds numbers less than $Re = 2500$ (Fig. 12(a)). Four horseshoe vortices were generated for Reynolds numbers equal to or higher than $Re = 4000$ (Fig. 12(b)), and two outside vortices were intermittent. All of the horseshoe vortices were generated intermittently over $Re = 6000$ (Fig. 12(c)). This intermittency is related to the behavior of alternate vortices as stated previously.

In Fig. 13, the pattern of the particles lying on the bottom of the heated wall is shown corresponding to the flow near the heated surface. Figures 14(a)–(c) show top views of the horseshoe vortices and these patterns on the wall.

The dark parts in Fig. 13 show that the particles do not accumulate in large amounts. This kind of pattern is considered to express the characteristics of flow corresponding to shear stress. For $Re = 1000$ (Fig.

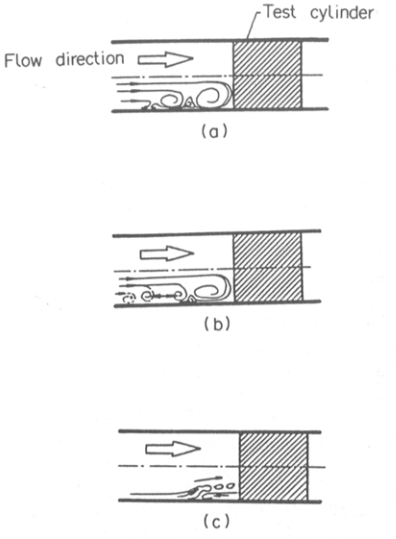

FIG. 12. The behavior of horseshoe vortices for various Reynolds numbers: (a) $Re = 1000$; (b) $Re = 4000$; (c) $Re = 10000$.

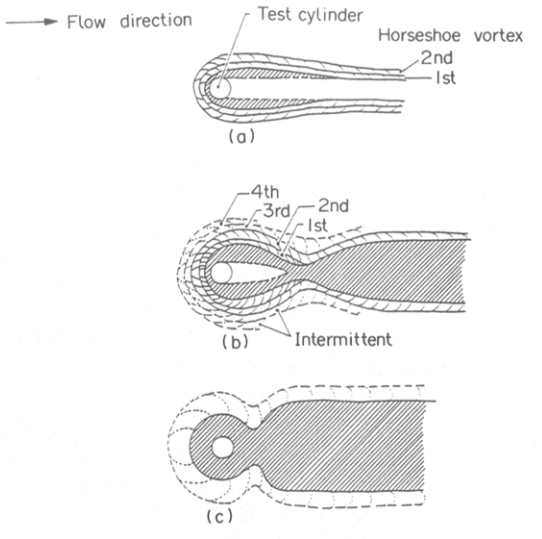

FIG. 14. A model of flow patterns for various Reynolds numbers: (a) $Re = 1000$; (b) $Re = 4000$; (c) $Re = 10000$.

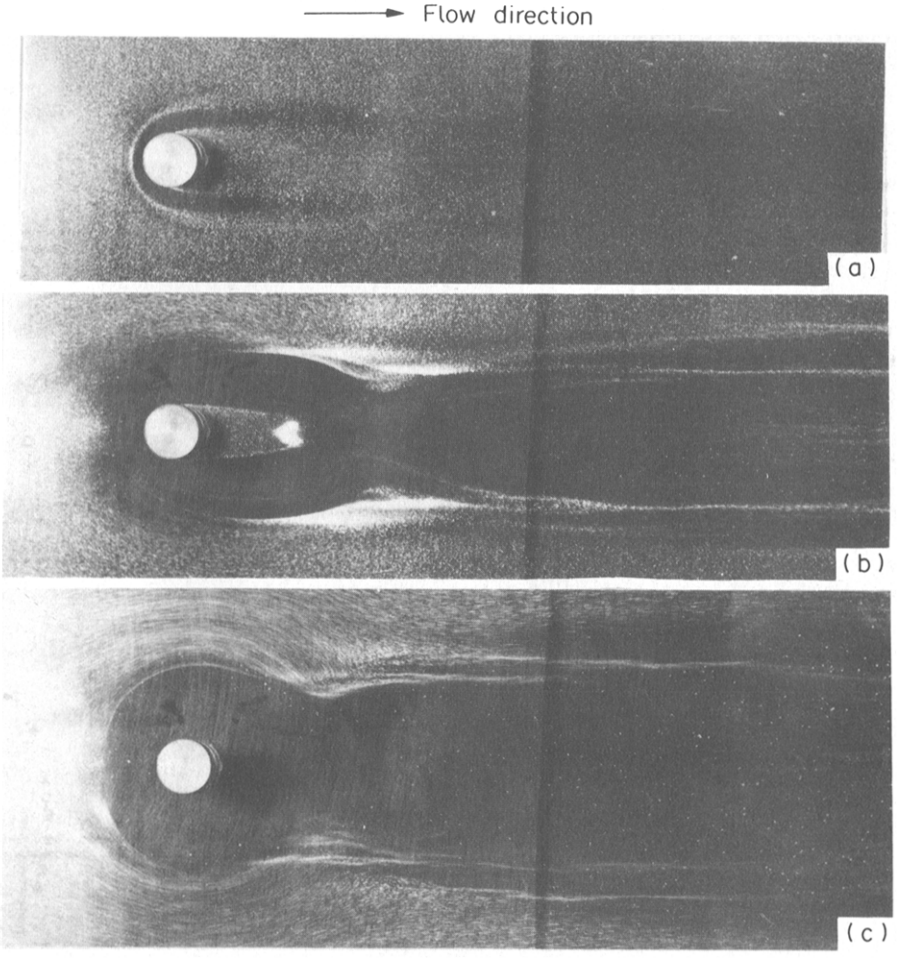

FIG. 13. Precipitation pattern of pearlized particles on the bottom plate (exposure, f8; time, 0.25 s): (a) $Re = 1000$; (b) $Re = 4000$; (c) $Re = 10000$.

13(a)), a curved white line represents the boundary of the outside horseshoe vortices near a cylindrical rod. For $Re = 4000$ (Fig. 13(b)), two curved white lines correspond to the outside boundary of two horseshoe vortices. In the downstream region, patterns of pearlized particles are observed corresponding to the stagnation region. The width of the pattern is reduced once, and then extended again to the flow direction. In Fig. 13(c), the photograph was taken by illuminating tangentially the slit of a light source along the wall and shows that the particles move downstream along the bottom wall with wavering. The size of patterns around a cylindrical rod reduces with an increase of Re, and the shape is similar to a circle. The width of the wake flow was primarily constant. This characteristic is a common representation of Reynolds numbers higher than $Re = 5000$. These patterns from a cylindrical rod to the stagnation region correspond well to the temperature distribution.

CONCLUDING REMARKS

The effects of a cylindrical rod (corresponding to a spacer) in a parallel plate duct on the heat transfer and the flow situation were determined experimentally.

(1) The effective area was clarified by visualizing the temperature of the liquid crystal sheet. Heat transfer was evaluated by the maximum and average Nusselt numbers and the characteristics were clarified. The most effective area of heat transfer augmentation existed downstream of a circular rod.

(2) The cylindrical rod made of brass with high thermal conductivity gave a 25% higher local heat transfer coefficient (due to the fin effect) than the cylindrical rod made of acrylic resin.

(3) Small pearlized particles were used to visualize the flow situation. Horseshoe vortices around a cylindrical rod contributed to the improvement of the local heat transfer of the wake flow.

These results will be extended to the study of several spacers and will be useful as fundamental data for practical application.

Acknowledgements—We would like to thank Dr H. Kawamura, Japan Atomic Energy Research Institute, who advised us to advance the study.

REFERENCES

1. M. Hiwada, T. Kawamura, T. Hibino, I. Mabuchi and M. Kumada, Heat transfer from the finite circular cylinder settled on the flat plate (in the case of the length of the cylinder larger than the thickness of the turbulence boundary layer), *Trans. J.S.M.E.* (*B*) 50–451, 733–741 (1984).
2. T. Kawamura, M. Hiwada, I. Mabuchi and M. Kumada, Augmentation of turbulent heat transfer on flat plate with a three-dimensional protuberance (1st Report, Local heat transfer characteristics and flow pattern around a finite length circular protuberance), *Trans. J.S.M.E.* (*B*) 50–452, 1034–1041 (1984).
3. M. Hiwada and I. Mabuchi, Fluid flow and heat transfer around a circular cylinder with high blockage ratio, *Trans. J.S.M.E.* (*B*) 46–409, 1750–1758 (1980).
4. K. Oyakawa and I. Mabuchi, Fluid flow and heat transfer in a parallel plate duct containing a cylinder, *Trans. J.S.M.E.* (*B*) 47–414, 308–315 (1981).
5. K. Oyakawa and I. Mabuchi, Heat transfer in a parallel plate duct with circular cylinder placed staggered, *Trans. J.S.M.E.* (*B*) 48–432, 1509–1517 (1982).
6. K. Kobayashi, *Liquid Crystal*, p. 75. Nikkan Kogyo Shinbun-Sha (1976).
7. N. Akino, K. Suzuki, K. Sanokawa and Y. Okamoto, Visualization of temperature and heat transfer distributions around a promoter in a parallel plate channel by thermosensitive liquid crystal film, *Flow Visualization* 3–8, 40–46 (1983).
8. O. Savaz, On flow visualization using reflective flakes, *J. Fluid Mech.* **152,** 235–248 (1985).
9. *JSME Data Book of Heat Transfer*, p. 28 (1978).
10. W. M. Kays, *Convective Heat and Mass Transfer*, p. 115. McGraw-Hill, New York (1966).
11. R. J. Goldstein, M. K. Chyu and R. C. Hain, Measurement of local mass transfer on a surface in the region of the base of a protruding cylinder with a computer-controlled data acquisition system, *Int. J. Heat Mass Transfer* **28,** 977–985 (1985).
12. P. P. Zemanick and R. S. Dougall, Local heat transfer downstream of abrupt circular channel expansion, *Trans. ASME*, Ser. C **89**(2), 53–60 (1970).
13. E. G. Filleti and W. M. Kays, Heat transfer in separated, reattached, and redevelopment region behind a double step at entrance to a flat duct, *Trans. ASME*, Ser. C **89**(2), 163–168 (1967).
14. C. J. Baker, The laminar horseshoe vortex, *J. Fluid Mech.* **95**(2), 347–367 (1979).

ETUDE FONDAMENTALE DE L'ECOULEMENT ET DU TRANSFERT DE CHALEUR AUTOUR D'UN ESPACEUR (DANS LE CAS D'UNE BARRE CYLINDRIQUE COMME ESPACEUR)

Résumé—On décrit l'accroissement du transfert thermique et l'écoulement autour d'un espaceur unique (une tige cylindrique) sur une surface chauffée d'un canal entre plans parallèles, de façon à préciser les effets de l'espaceur dans les éléments combustibles d'un réacteur à haute température refroidi au gaz. Les extrémités de la tige cylindrique touchent les plans supérieur et inférieur. Un film de cristal liquide thermosensible est utilisé pour montrer l'aire effective du transfert de chaleur. Le nombre de Nusselt moyen qui est estimé, présente un pic à la distance adimensionnelle $X/D = 1$–3, puis il décroît graduellement dans la direction de l'écoulement. On examine aussi la façon dont le transfert thermique correspond à la configuration de l'écoulement. Le tourbillon en fer à cheval produit autour de l'espaceur, affecte le sillage et contribue à l'accroissement local du transfert de chaleur.

GRUNDLEGENDE UNTERSUCHUNG VON WÄRMEÜBERGANG UND STRÖMUNG UM EINEN ZYLINDRISCHEN STAB ALS ABSTANDHALTER

Zusammenfassung—Es wird die Verbesserung des Wärmeübergangs sowie die Strömung um einen einzelnen zylindrischen Stab als Abstandshalter auf einer beheizten Oberfläche eines durch parallele Platten gebildeten Strömungskanals beschrieben, um die Effekte der Abstandshalter in den Brennelementen eines gasgekühlten Hochtemperaturreaktors grundlegend zu untersuchen. Die Enden des zylindrischen Stabes berühren die obere und untere Platte. Ein wärmeempfindlicher Flüssigkristallfilm wird dazu benutzt, das effektive Gebiet der Wärmeübertragung zu markieren. Die mittlere Nusselt-Zahl, die für ein bestimmtes Gebiet stromab vom Abstandhalter berechnet wird, hat einen Höchstwert bei der dimensionslosen Entfernung von $X/D = 1$–3; danach nimmt sie allmählich in Strömungsrichtung ab. In welcher Weise Wärmeübergang und Strömung zusammenhängen wird ebenfalls untersucht. Der durch den Abstandhalter erzeugte Hufeisen-Wirbel bewirkt einen Nachlauf und trägt zum Anwachsen der örtlichen Wärmeübertragung bei.

ФУНДАМЕНТАЛЬНОЕ ИССЛЕДОВАНИЕ ТЕПЛООБМЕНА И ОБТЕКАНИЯ ЦИЛИНДРИЧЕСКОЙ РАСПОРКИ

Аннотация—Проведено исследование интенсификации теплообмена и картины обтекания единичной распорки (цилиндрического стержня) на нагреваемой поверхности канала из параллельных пластин. Исследование выполнено с целью выяснения влияния распорок в твэлах высокотемпературного газоохлаждаемого реактора. Торцы цилиндрического стержня соприкасаются с верхней и нижней стенками канала. Эффективная площадь переноса тепла определяется с помощью термочувствительной жидкокристаллической пленки. Среднее значение числа Нуссельта, определяемое на некотором удалении от распорок вниз по течению, достигает максимального значения на расстоянии (безразмерном) $X/D = 1$–3, а затем постепенно снижается вниз по потоку. Также исследуется взаимосвязь между теплопереносом и течением. Возникающие вокруг распорки подковообразные вихри возмущают след за распоркой и способствует увеличению локального переноса тепла.